ELSEVIER

Journal of Fluids and Structures 22 (2006) 647–661

JOURNAL OF FLUIDS AND STRUCTURES

www.elsevier.com/locate/jfs

Slow motion of a slip spherical particle perpendicular to two plane walls

Y.C. Chang, H.J. Keh*

Department of Chemical Engineering, National Taiwan University, Taipei 10617, Taiwan, ROC

Received 14 April 2005; accepted 17 February 2006
Available online 4 May 2006

Abstract

The problem of the quasisteady motion of a spherical fluid or solid particle with a slip-flow surface in a viscous fluid perpendicular to two parallel plane walls at an arbitrary position between them is investigated theoretically in the limit of small Reynolds number. To solve the axisymmetric Stokes equation for the fluid velocity field, a general solution is constructed from the superposition of the fundamental solutions in both circular cylindrical and spherical coordinate systems. The boundary conditions are enforced first at the plane walls by the Hankel transform and then on the particle surface by a collocation technique. Numerical results for the hydrodynamic drag force exerted on the particle are obtained with good convergence for various values of the relative viscosity or slip coefficient of the particle and of the relative separation distances between the particle and the confining walls. For the motions of a spherical particle normal to a single plane wall and of a no-slip sphere perpendicular to two plane walls, our drag results are in good agreement with the available solutions in the literature for all relative particle-to-wall spacings. The boundary-corrected drag force acting on the particle in general increases with an increase in its relative viscosity or with a decrease in its slip coefficient for a given geometry, but there are exceptions. For a specified wall-to-wall spacing, the drag force is minimal when the particle is situated midway between the two plane walls and increases monotonically when it approaches either of the walls. The boundary effect on the particle motion normal to two plane walls is found to be significant and much stronger than that parallel to them.

Keywords: Creeping flow; Fluid droplet; Aerosol sphere; Slip-flow surface; Drag force; Boundary effect

1. Introduction

Problems concerning the migration of solid particles or fluid droplets through a viscous fluid at very small Reynolds numbers have continued to receive much attention from investigators in the fields of chemical, biomedical, and environmental engineering and science. The majority of these moving phenomena is fundamental in nature, but permits one to develop rational understanding of many practical systems and industrial processes such as sedimentation, flotation, coagulation, meteorology, motion of blood cells in an artery or vein, rheology of suspensions, and colloidal studies. The theoretical study of this subject has grown out of the classic work of Stokes (1851) for a translating, no-slip, rigid sphere in a viscous fluid.

*Corresponding author. Tel.: +886 2 33663 048; fax: +886 2 2362 3040.
E-mail address: huan@ntu.edu.tw (H.J. Keh).

0889-9746/$ - see front matter © 2006 Elsevier Ltd. All rights reserved.
doi:10.1016/j.jfluidstructs.2006.02.006

Hadamard (1911) and Rybczynski (1911) extended independently Stokes' analysis to the translation of a fluid sphere in a second, immiscible fluid. Assuming continuous velocity and continuous tangential stress across the interface between the fluid phases, they found that the force acting on a spherical droplet of radius a by the ambient fluid of viscosity η is

$$\mathbf{F}_0 = -6\pi\eta a \frac{3\eta^* + 2}{3\eta^* + 3}\mathbf{U}, \tag{1}$$

where $\mathbf{U}$ is the migration velocity of the droplet and η^* is the internal-to-external viscosity ratio. Since the fluid properties are arbitrary, Eq. (1) degenerates to the case of translation of a solid sphere (Stokes' law) when $\eta^* \to \infty$ and to the case of motion of a gas bubble with spherical shape in the limit $\eta^* \to 0$.

When one tries to solve the Navier–Stokes equation, it is usually assumed that no slippage arises at the solid–fluid interfaces. Actually, this is an idealization of occurrence of the transport processes. The phenomenon that the adjacent fluid (especially if the fluid is a slightly rarefied gas) can slip over a solid surface has been confirmed, both experimentally and theoretically (Kennard, 1938; Ying and Peters, 1991; Hutchins et al., 1995). Presumably, any such slipping would be proportional to the local velocity gradient next to the solid surface (see Eq. (18)), at least so long as this gradient is small (Happel and Brenner, 1983). The constant of proportionality, β^{-1}, may be termed a "slip coefficient". Basset (1961) found that the force exerted by the surrounding fluid on a translating rigid sphere with a slip-flow boundary condition at its surface (e.g., a settling aerosol sphere) is

$$\mathbf{F}_0 = -6\pi\eta a \frac{\beta a + 2\eta}{\beta a + 3\eta}\mathbf{U}, \tag{2}$$

where $\mathbf{U}$ is the translational velocity of the particle. In the particular case of $\beta \to \infty$, there is no slip at the particle surface and Eq. (2) degenerates to Stokes' law. When $\beta = 0$, there is a perfect slip at the particle surface and Eq. (2) is consistent with Eq. (1) (taking $\eta^* = 0$). Note that, as can be seen from Eqs. (1) and (2), the unbounded flow field caused by the migration of a "slip" solid sphere is the same as the external flow field generated by the same motion of a spherical fluid droplet with a value of η^* equal to the parameter $\beta a/3\eta$ of the solid sphere.

In Eq. (2), the slip coefficient has been determined experimentally for various cases and found to agree with the general kinetic theory of gases. It can be calculated from the formula

$$\frac{\eta}{\beta} = C_m l, \tag{3}$$

where l is the mean free path of a gas molecule and C_m is a dimensionless constant related to the momentum accommodation coefficient at the solid surface. Although C_m surely depends upon the nature of the surface, examination of the experimental data suggests that it will be in the range 1.0–1.5 (Davis, 1972; Talbot et al., 1980; Loyalka, 1990). The slip-flow boundary condition is generally applicable in the continuum regime (with the Knudsen number $l/a \ll 1$). The quantity η/β is a length, which can be pictured by noting that the fluid motion is the same as if the solid surface was displaced inward by a distance η/β with the velocity gradient extending uniformly right up to no-slip velocity at the surface.

In most practical applications of low-Reynolds-number motions, particles or droplets are not isolated (Keh and Tseng, 1992; Keh and Chen, 1997) and the surrounding fluid is externally bounded by solid walls. Thus, it is important to determine if the presence of neighboring boundaries significantly affects the movement of a particle or droplet. Using spherical bipolar coordinates, Bart (1968) and Rushton and Davies (1973) examined the motion of a spherical fluid droplet settling normal to a plane interface between two immiscible viscous fluids. This work is an extension of the analyses of Maude (1961) and Brenner (1961), who independently analyzed the fluid motion generated by a no-slip sphere moving perpendicular to a solid plane surface or to a free-surface plane. Wacholder and Weihs (1972) also utilized bipolar coordinates to study the motion of a fluid sphere through another fluid normal to a no-slip or free plane surface; their calculations agree with the results obtained by Bart in these limits. Hetsroni et al. (1970) used a method of reflections to solve for the terminal settling velocity of a spherical fluid droplet moving axially at an arbitrary radial location within a long circular tube filled with a viscous fluid. The wall effects experienced by a fluid sphere moving along the axis of a circular tube were also examined by using a reciprocal theorem (Brenner, 1971) and an approximative approach (Coutanceau and Thizon, 1981). The parallel motion of a spherical droplet in a quiescent immiscible fluid at an arbitrary position between two parallel plane walls was studied by Shapira and Haber (1988) using the method of reflections and by Keh and Chen (2001) using a boundary collocation technique. Approximate analytical solutions and exact numerical solutions for the hydrodynamic drag force acting on the fluid droplet were obtained as functions of η^*, a/b, and $a/(b+c)$, where b and c are the respective distances from the droplet center to the two plane walls.

The boundary effects on solid particles with finite values of $\beta a/\eta$ are different, both physically and mathematically, from those on fluid droplets of finite viscosities. Through an exact representation in spherical bipolar coordinates, Reed and Morrison (1974) and Chen and Keh (1995) examined the creeping motion of a rigid sphere normal to an infinite plane wall, where the fluid may slip at the solid surfaces. Later, the quasisteady translation of a slip spherical particle in a spherical cavity was also theoretically studied (Keh and Chang, 1998; Lu and Lee, 2001). An analytical expression for the wall-corrected drag force exerted on the particle located at the center of the cavity was derived in a closed form. Recently, the slow translational and rotational motions of a slip sphere along the symmetric axis of a circular cylindrical pore (Lu and Lee, 2002) and parallel to two plane walls at an arbitrary position between them (Chen and Keh, 2003) have been investigated with the use of the boundary collocation method. Numerical results for the hydrodynamic drag force and torque acting on the particle were obtained for various cases.

The purpose of this article is to obtain exact solutions for the slow translational motion of a spherical fluid or solid particle with a slip surface perpendicular to two parallel plane walls at an arbitrary position between them. The creeping-flow equations applicable to the systems are solved by using a combined analytical–numerical method with the boundary collocation technique (Ganatos et al., 1980), and the wall-corrected drag force acting on the particle is obtained with good convergence for various cases. For the special cases of movement of a spherical particle with a no-slip surface and/or normal to a single plane wall, our calculations show excellent agreement with the available solutions in the literature. Because the governing equations and boundary conditions concerning the general problem of motion of a particle at an arbitrary position between two parallel plane walls in an arbitrary direction are linear, its solution can be obtained as a superposition of the solutions for its two subproblems: motion parallel to the plane walls, which was previously examined (Keh and Chen, 2001; Chen and Keh, 2003), and motion normal to the confining walls, which is treated in this work.

2. Formulation for the motion of a spherical fluid droplet perpendicular to two plane walls

In this section, we consider the quasisteady creeping motion caused by a fluid sphere of radius a translating with a constant velocity $\mathbf{U} = U\mathbf{e}_z$ in a second, immiscible fluid perpendicular to two infinite parallel plane walls whose distances from the center of the droplet are b and c, as shown in Fig. 1. Here (ρ, ϕ, z) and (r, θ, ϕ) denote the circular cylindrical and spherical coordinate systems, respectively, with the origin of coordinates at the droplet center, and $\mathbf{e}_z$ is the unit vector in the z direction. We set $b \leqslant c$ throughout this work, without the loss of generality. The droplet is assumed to be sufficiently small so that interfacial tension (which is assumed to be fairly large) maintains its spherical shape. The external fluid is at rest far away from the droplet. The objective is to determine the correction to Eq. (1) for the motion of the droplet due to the presence of the plane walls.

The fluids inside and outside the droplet are assumed to be incompressible and Newtonian. Owing to the low Reynolds number, the fluid motion is governed by the quasisteady fourth-order differential equations for viscous axisymmetric creeping flows,

$$E^2(E^2\Psi) = 0 \quad (r \geqslant a), \tag{4a}$$

$$E^2(E^2\Psi_1) = 0 \quad (r \leqslant a), \tag{4b}$$

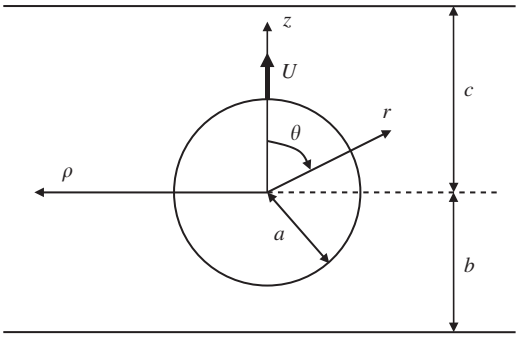

Fig. 1. Geometric sketch of the translation of a spherical droplet perpendicular to two plane walls at an arbitrary position between them.

where Ψ_1 and Ψ are the Stokes stream functions for the flow inside the droplet and for the external flow, respectively, which are related to their corresponding velocity components in cylindrical coordinates by

$$v_\rho = \frac{1}{\rho}\frac{\partial \Psi}{\partial z}, \tag{5a}$$

$$v_z = -\frac{1}{\rho}\frac{\partial \Psi}{\partial \rho} \tag{5b}$$

and the Stokes operator E^2 has the form

$$E^2 = \rho \frac{\partial}{\partial \rho}\left(\frac{1}{\rho}\frac{\partial}{\partial \rho}\right) + \frac{\partial^2}{\partial z^2}. \tag{6}$$

The boundary conditions for the fluid velocities at the droplet surface, where both velocity and shear stress are continuous, on the plane walls, and far removed from the droplet are

$$r = a : v_\rho = v_{1\rho}, \tag{7a}$$

$$v_z = v_{1z}, \tag{7b}$$

$$v_\rho \tan\theta + v_z = U, \tag{7c}$$

$$\tau_{r\theta} = \tau_{1r\theta}, \tag{7d}$$

$$z = c, -b : v_\rho = v_z = 0, \tag{8}$$

$$\rho \to \infty : v_\rho = v_z = 0. \tag{9}$$

Here, $\tau_{r\theta}$ and $\tau_{1r\theta}$ are the viscous stresses for the external flow and the flow inside the droplet, respectively.

To solve the external flow field, we express the stream function in the form (Ganatos et al., 1980)

$$\Psi = \Psi_w + \Psi_p. \tag{10}$$

Here Ψ_w is a separable solution of Eq. (4a) in cylindrical coordinates that represents the disturbance produced by the plane walls and is given by a Fourier–Bessel integral

$$\Psi_w = \int_0^\infty [A(\omega)e^{\omega z} + B(\omega)e^{-\omega z} + C(\omega)\omega z e^{\omega z} + D(\omega)\omega z e^{-\omega z}]\rho J_1(\omega\rho)\,d\omega, \tag{11}$$

where $A(\omega)$, $B(\omega)$, $C(\omega)$, and $D(\omega)$ are unknown functions of the separation variable ω. The second part of Ψ, denoted by Ψ_p, is a separable solution of Eq. (4a) in spherical coordinates representing the disturbance generated by the droplet and is given by

$$\Psi_p = \sum_{n=2}^{\infty}\left(B_n r^{-n+1} + D_n r^{-n+3}\right) G_n^{-1/2}(\cos\theta), \tag{12}$$

where $G_n^{-1/2}$ is the Gegenbauer polynomial of the first kind of order n and degree $-\frac{1}{2}$; B_n and D_n are unknown constants. Note that the boundary condition in Eq. (9) is immediately satisfied by a solution of the form given by Eqs. (10)–(12).

The general solution to Eq. (4b) for the internal flow field can be expressed as

$$\Psi_1 = \sum_{n=2}^{\infty}\left(A_n r^n + C_n r^{n+2}\right) G_n^{-1/2}(\cos\theta), \tag{13}$$

or

$$v_{1\rho} = \sum_{n=2}^{\infty}\left[A_n \alpha_{1n}^{(1)}(r,\theta) + C_n \alpha_{2n}^{(1)}(r,\theta)\right], \tag{14a}$$

$$v_{1z} = \sum_{n=2}^{\infty}\left[A_n \alpha_{1n}^{(2)}(r,\theta) + C_n \alpha_{2n}^{(2)}(r,\theta)\right], \tag{14b}$$

where the definitions of the functions $\alpha_{in}^{(j)}(r,\theta)$ for i and j equal to 1 or 2 are given by Eqs. (A.1) and (A.2) in Appendix A, and A_n and C_n are unknown constants. A solution of this form satisfies the requirement that the velocity is finite for any position within the droplet.

Substituting the stream function Ψ given by Eqs. (10)–(12) into the boundary conditions in Eq. (8) and applying the Hankel transform on the variable ρ lead to a solution for the functions $A(\omega)$, $B(\omega)$, $C(\omega)$, and $D(\omega)$ in terms of the coefficients B_n and D_n. After the substitution of this solution into Eqs. (10)–(12), the fluid velocity components can be expressed as

$$v_\rho = \sum_{n=2}^{\infty}\left[B_n\gamma_{1n}^{(1)}(r,\theta) + D_n\gamma_{2n}^{(1)}(r,\theta)\right], \tag{15a}$$

$$v_z = \sum_{n=2}^{\infty}\left[B_n\gamma_{1n}^{(2)}(r,\theta) + D_n\gamma_{2n}^{(2)}(r,\theta)\right], \tag{15b}$$

where the definitions of the functions $\gamma_{in}^{(j)}(r,\theta)$ for i and j equal to 1 or 2 are given by Eqs. (A.3) and (A.4) (in integral forms which must be evaluated numerically).

The only boundary conditions that remain to be satisfied are those on the droplet surface. Substituting Eqs. (14) and (15) into Eq. (7), one obtains

$$\sum_{n=2}^{\infty}\left[B_n\gamma_{1n}^{(1)}(a,\theta) + D_n\gamma_{2n}^{(1)}(a,\theta) - A_n\alpha_{1n}^{(1)}(a,\theta) - C_n\alpha_{2n}^{(1)}(a,\theta)\right] = 0, \tag{16a}$$

$$\sum_{n=2}^{\infty}\left[B_n\gamma_{1n}^{(2)}(a,\theta) + D_n\gamma_{2n}^{(2)}(a,\theta) - A_n\alpha_{1n}^{(2)}(a,\theta) - C_n\alpha_{2n}^{(2)}(a,\theta)\right] = 0, \tag{16b}$$

$$\sum_{n=2}^{\infty}\left\{B_n\left[\gamma_{1n}^{(1)}(a,\theta)\tan\theta + \gamma_{1n}^{(2)}(a,\theta)\right] + D_n\left[\gamma_{2n}^{(1)}(a,\theta)\tan\theta + \gamma_{2n}^{(2)}(a,\theta)\right]\right\} = U, \tag{16c}$$

$$\sum_{n=2}^{\infty}\left[B_n\gamma_{1n}^{*}(a,\theta) + D_n\gamma_{2n}^{*}(a,\theta) - \eta^* A_n\alpha_{1n}^{*}(a,\theta) - \eta^* C_n\alpha_{2n}^{*}(a,\theta)\right] = 0, \tag{16d}$$

where the functions $\alpha_{in}^{*}(r,\theta)$ and $\gamma_{in}^{*}(r,\theta)$ for $i = 1$ or 2 are defined by Eqs. (A.13) and (A.14) (in which the integration must be performed numerically).

To satisfy the conditions in Eq. (16) exactly along the entire surface of the droplet would require the solution of the entire infinite array of unknown constants A_n, C_n, B_n, and D_n. However, the collocation method (O'Brien, 1968; Ganatos et al., 1980; Keh and Chen, 2001) enforces the boundary conditions at a finite number of discrete points on the semi-circular longitudinal arc of the sphere (from $\theta = 0$ to π) and truncates the infinite series in Eqs. (13)–(15) into finite ones. If the spherical boundary is approximated by satisfying the conditions in Eq. (7) at N discrete points on the generating arc, the infinite series in Eqs. (13)–(15) are truncated after N terms, resulting in a system of $4N$ simultaneous linear algebraic equations in the truncated form of Eq. (16). This matrix equation can be numerically solved to yield the $4N$ unknown constants A_n, C_n, B_n, and D_n required in the truncated form of Eqs. (14) and (15). The fluid velocity field is completely obtained once these coefficients are solved for a sufficiently large number of N. The accuracy of the boundary-collocation/truncation technique can be improved to any degree by taking a sufficiently large value of N. Naturally, as $N\to\infty$ the truncation error vanishes and the overall accuracy of the solution depends only on the numerical integration required in evaluating the functions $\gamma_{in}^{(j)}$ and γ_{in}^{*} in Eq. (16).

The drag force $\mathbf{F} = F\mathbf{e}_z$ exerted by the fluid on the droplet can be determined from (Happel and Brenner, 1983)

$$F = 4\pi\eta D_2. \tag{17}$$

This expression shows that only the lowest-order coefficient D_2 contributes to the hydrodynamic force acting on the droplet.

3. Solutions for the motion of a spherical fluid droplet perpendicular to two plane walls

The numerical results for the creeping motion of a spherical droplet of an arbitrary viscosity perpendicular to two plane walls at an arbitrary position between them, obtained by using the boundary collocation method described in the

previous section, are presented in this section. The system of linear algebraic equations to be solved for the coefficients A_n, C_n, B_n, and D_n is constructed from Eq. (16). All the numerical integrations to evaluate the functions $\gamma_{in}^{(j)}$ and γ_{in}^{*} were done by the 180-point Gauss–Laguerre quadrature.

When specifying the points along the half-circular generating arc of the fluid sphere (with a constant value of ϕ) where the boundary conditions are to be exactly satisfied, the first points that should be chosen are $\theta = 0$ and π, since these points control the gaps between the droplet and the plane walls. In addition, the point $\theta = \pi/2$ which defines the projected area of the droplet normal to the direction of motion is also important. However, an examination of the system of linear algebraic equations in Eq. (16) shows that the matrix equations become singular if these points are used. To overcome this difficulty, these points are replaced by closely adjacent points, i.e., $\theta = \delta$, $\pi/2-\delta$, $\pi/2+\delta$, and $\pi-\delta$ (Ganatos et al., 1980). Additional points along the boundary are selected as mirror-image pairs about the plane $\theta = \pi/2$ to divide the two quarter-circular arcs of the droplet into equal segments. The optimum value of δ in this work is found to be 0.01°, with which the numerical results of the hydrodynamic drag force acting on the particle converge satisfactorily.

In Table 1, the collocation solutions for the hydrodynamic drag force exerted on a fluid sphere moving perpendicular to a single plane wall (with $c \to \infty$) for various values of a/b and η^* are presented. The drag force F_0 acting on an identical droplet in an unbounded fluid, given by Eq. (1) (with $\mathbf{F}_0 = F_0\mathbf{e}_z$), is used to normalize the boundary-corrected values. Obviously, $F/F_0 = 1$ as $a/b = 0$ for any value of η^*. The accuracy and convergence behavior of the truncation technique depends principally upon the ratio a/b. All of the results obtained under this collocation scheme converge to at least five significant figures. For the difficult case of $a/b = 0.999$, the number of collocation points $N = 200$ is sufficiently large to achieve this convergence. Our collocation results agree excellently with the numerical solutions obtained by Bart (1968) using spherical bipolar coordinates. As expected, the results in Table 1 illustrate that the drag force on the droplet is a monotonic increasing function of a/b, and will become infinite in the limit $a/b = 1$, for any given value of η^*. In general, the normalized wall-corrected drag force on the droplet increases monotonically with an increase in η^*, keeping a/b unchanged. Interestingly, when the value of a/b is very close to unity (say, greater than about 0.995), F/F_0 first decreases with an increase in η^* from $\eta^* = 0$, reaches a minimum at some finite value of η^*, and then increases with increasing η^* to the limit $\eta^* \to \infty$.

Some converged collocation solutions for the normalized drag force F/F_0 are presented in Table 2 for the motion of a spherical droplet perpendicular to two plane walls at two particular positions between them (with $b/(b+c) = 0.25$ and 0.5) for various values of a/b and η^*. For the special case of a rigid sphere (with $\eta^* \to \infty$), our results agree well with the previous solutions obtained by a method of reflection (Ho and Leal, 1974) and by a similar collocation method (Ganatos et al, 1980). Analogous to the situation of translation of a fluid sphere normal to a single plane wall, for a constant value of $b/(b+c)$, Table 2 indicates that the normalized drag force on the droplet increases monotonically with an increase in a/b (again, $F/F_0 = 1$ as $a/b = 0$ and $F/F_0 \to \infty$ as $a/b \to 1$) for a fixed value of η^* and with an increase in η^* for a given value of a/b not too close to unity.

Table 1
The normalized drag force F/F_0 experienced by a spherical droplet translating normal to a single plane wall at various values of a/b and η^*

a/b	F/F_0			
	$\eta^* = 0$	$\eta^* = 1$	$\eta^* = 10$	$\eta^* = \infty$
0.1	1.08110	1.10318	1.12194	1.12619
0.2	1.17678	1.22849	1.27440	1.28509
0.3	1.29224	1.38300	1.46801	1.48843
0.4	1.43611	1.57854	1.72084	1.75635
0.5	1.62382	1.83605	2.06544	2.12554
0.6	1.88574	2.19600	2.56622	2.66954
0.7	2.29122	2.74848	3.37017	3.55939
0.8	3.04340	3.74759	4.90393	5.30532
0.9	5.13001	6.35713	9.18424	10.44054
0.95	9.08847	10.91225	17.01655	20.57616
0.975	16.79597	19.10329	31.23217	40.71269
0.99	39.57004	41.44260	68.66238	100.8942
0.995	77.27764	76.32880	123.3256	201.0327
0.999	377.07	336.411	472.695	998.69

Table 2
The normalized drag force F/F_0 experienced by a spherical droplet translating normal to two parallel plane walls at various values of a/b, $b/(b+c)$, and η^*

$b/(b+c)$	a/b	F/F_0			
		$\eta^*=0$	$\eta^*=1$	$\eta^*=10$	$\eta^*=\infty$
0.25	0.1	1.08227	1.10471	1.12378	1.12811
	0.2	1.17957	1.23227	1.27912	1.29003
	0.3	1.29716	1.38994	1.47699	1.49792
	0.4	1.44384	1.58980	1.73590	1.77240
	0.5	1.63518	1.85300	2.08885	2.15071
	0.6	1.90172	2.22023	2.60069	2.70697
	0.7	2.31303	2.78178	3.41890	3.61288
	0.8	3.07247	3.79189	4.97052	5.37938
	0.9	5.16808	6.41435	9.27241	10.54051
	0.95	9.13181	10.97649	17.11657	20.69145
	0.975	16.84214	19.17105	31.33795	40.83617
	0.99	39.61798	41.51236	68.77117	101.0227
	0.995	77.32619	76.39922	123.4350	201.1630
	0.999	377.11	336.482	472.805	998.83
0.5	0.1	1.10714	1.13710	1.16285	1.16873
	0.2	1.23999	1.31374	1.38097	1.39686
	0.3	1.40911	1.54473	1.67728	1.70994
	0.4	1.63182	1.85358	2.08858	2.14942
	0.5	1.93887	2.28109	2.67966	2.78920
	0.6	2.39076	2.90613	3.57787	3.77653
	0.7	3.12597	3.90534	5.07385	5.45347
	0.8	4.55048	5.78039	8.01261	8.84044
	0.9	8.63955	10.84416	16.39942	19.00351
	0.95	16.51271	19.85195	31.92101	39.22095
	0.975	31.90530	36.16910	60.22857	79.46650
	0.99	77.44030	80.79911	134.9544	199.8128
	0.995	152.85	150.5510	244.202	400.085
	0.999	752.47	670.721	942.851	1995.46

Fig. 2 shows the collocation results for the hydrodynamic drag force exerted on a gas bubble (with $\eta^*\to 0$) moving perpendicular to two plane walls at various position between them. The dashed curves (with $a/b=$ constant) illustrate the effect of the position of the second wall (at $z=c$) on the drag force for various values of the relative sphere-to-wall spacing b/a. The solid curves (with $2a/(b+c)=$ constant) indicate the variation of the drag as a function of the bubble position at various values of the relative wall-to-wall spacing $(b+c)/2a$. At a constant value of $2a/(b+c)$, analogous to the corresponding case of a solid sphere (Ganatos et al., 1980), the bubble (or a droplet with a finite value of η^*, whose result is not exhibited here but can also be obtained accurately) experiences a minimum drag when it is located midway between the two walls (with $c=b$), and the drag force increases monotonically as the bubble or droplet approaches either of the walls.

In Fig. 3, the normalized drag force acting on a spherical droplet situated midway between two parallel plane walls (with $c=b$) undergoing perpendicular translation is plotted by solid curves as a function of a/b for various values of η^*. The corresponding drag on the droplet when the second wall is not present (with $c\to\infty$) is also plotted by dashed curves in the same figure for comparison. It can be seen from this figure (or from a comparison between Tables 1 and 2) that, for an arbitrary combination of parameters a/b and η^*, the assumption that the results for two walls can be obtained by simple addition of the single-wall effects always overestimates the correction to the hydrodynamic drag on a droplet.

Because the governing equations and boundary conditions for the general problem of creeping motion of a droplet in an arbitrary direction between two parallel plane walls are linear, the net solution can be obtained as a superposition of the solutions for its two subproblems: motion perpendicular to the plane walls, which is examined in this paper, and motion parallel to the confining boundaries. The collocation solutions for the slow motion of a spherical droplet

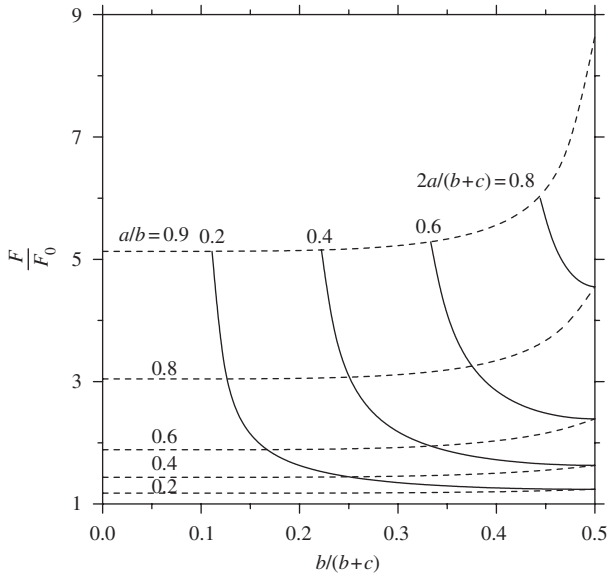

Fig. 2. Plots of the normalized drag force F/F_0 on a spherical gas bubble (with $\eta^* \to 0$) translating perpendicular to two plane walls versus the ratio $b/(b+c)$ with a/b and $2a/(b+c)$ as parameters.

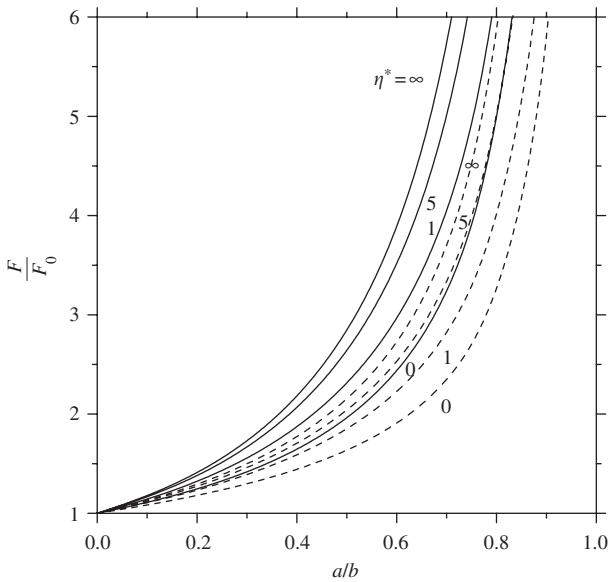

Fig. 3. Plots of the normalized drag force F/F_0 on a spherical droplet situated midway between two parallel plane walls (with $c = b$) undergoing perpendicular translation versus the ratio a/b with η^* as a parameter. The dashed curves are plotted for the translation of an identical droplet normal to a single plane wall for comparison.

parallel to two plane walls have already been obtained (Keh and Chen, 2001), and it was found that the wall-corrected normalized drag force acting on the droplet also increases with an increase in the viscosity ratio η^*. A comparison between those results and our solutions indicates that, as expected, the plane walls exert the most influence (or greatest drag) on the droplet when its migration occurs normal to them, and the least in the case of motion parallel to them. Their difference can be quite significant when the spacings between the droplet and the confining boundaries are small.

Therefore, the direction of migration of a fluid sphere at a position between two parallel plane walls is different from that of the applied force, except when it is oriented parallel or perpendicular to the plane walls.

4. Formulation for the motion of a slip solid sphere perpendicular to two plane walls

The quasisteady creeping motion caused by a solid spherical particle of radius a translating with a velocity $\mathbf{U} = U\mathbf{e}_z$ in a quiescent incompressible and Newtonian fluid perpendicular to two infinite parallel plane walls whose distances from the center of the particle are b and c, as shown in Fig. 1, is considered in this section. The Knudsen number l/a is assumed to be small so that the fluid flow is in the continuum regime. The objective is to determine the correction to Eq. (2) for the motion of the particle due to the presence of the plane walls.

The governing equation, the boundary conditions at the plane walls and at infinity, and the sufficiently general solution for the fluid flow are still given by Eqs. (4a), (8), (9), and (15). Now, the boundary conditions for the fluid velocity at the particle surface become (Basset, 1961; Happel and Brenner, 1983)

$$r = a: \quad v_\rho = \frac{1}{\beta}\tau_{r\theta}\cos\theta, \tag{18a}$$

$$v_z = U - \frac{1}{\beta}\tau_{r\theta}\sin\theta, \tag{18b}$$

where $1/\beta$ is the frictional slip coefficient about the surface of the particle. Substituting Eq. (15) into Eq. (18), one obtains

$$\sum_{n=2}^{\infty}\left\{B_n\left[\gamma_{1n}^{(1)}(a,\theta) - \frac{\eta}{\beta}\gamma_{1n}^{*}(a,\theta)\cos\theta\right] + D_n\left[\gamma_{2n}^{(1)}(a,\theta) - \frac{\eta}{\beta}\gamma_{2n}^{*}(a,\theta)\cos\theta\right]\right\} = 0, \tag{19a}$$

$$\sum_{n=2}^{\infty}\left\{B_n\left[\gamma_{1n}^{(2)}(a,\theta) + \frac{\eta}{\beta}\gamma_{1n}^{*}(a,\theta)\sin\theta\right] + D_n\left[\gamma_{2n}^{(2)}(a,\theta) + \frac{\eta}{\beta}\gamma_{2n}^{*}(a,\theta)\sin\theta\right]\right\} = U, \tag{19b}$$

where the functions $\gamma_{in}^{(j)}(r,\theta)$ and $\gamma_{in}^{*}(r,\theta)$ for i and j equal to 1 or 2 have been defined by Eqs. (A.3), (A.4), and (A.14).

Eq. (19) can also be satisfied by utilizing the boundary collocation technique presented in Section 2 for the solution about a migrating droplet. At the particle surface, Eq. (19) is applied at N discrete points (values of θ between 0 and π) and the infinite series in Eq. (15) are truncated after N terms. This generates a set of $2N$ linear algebraic equations for the $2N$ unknown constants B_n and D_n. The fluid velocity field is completely obtained once these coefficients are solved for a sufficiently large number of N. Again, the hydrodynamic drag force $\mathbf{F} = F\mathbf{e}_z$ acting on the spherical particle can be determined from Eq. (17).

5. Solutions for the motion of a slip solid sphere perpendicular to two plane walls

In Section 3 collocation solutions for the migration of a fluid sphere perpendicular to two plane walls at an arbitrary position between them have been presented and were found to be in excellent agreement with the available solutions for the limiting cases. This section will examine the solutions for the corresponding motion of a slip solid sphere using the same collocation method. Now, the system of linear algebraic equations to be solved for the coefficients B_n and D_n is constructed from Eq. (19).

The collocation solutions of the hydrodynamic drag force acting on a spherical particle translating normal to a plane wall (with $c \to \infty$) for different values of the parameters $\beta a/\eta$ and a/b are presented in Table 3. Here, the drag force F_0 exerted on an identical particle in an unbounded fluid given by Eq. (2) (with $\mathbf{F}_0 = F_0\mathbf{e}_z$) is used to normalize the boundary-corrected values. Evidently, $F/F_0 = 1$ as $a/b = 0$ for any value of $\beta a/\eta$. All of the results obtained under the collocation scheme converge satisfactorily to at least the significant figures shown in the table. For the special cases of translation of a no-slip sphere (with $\beta a/\eta \to \infty$) and of a perfectly slip sphere (with $\beta a/\eta = 0$) normal to a plane wall, our numerical results are exactly the same as those presented in Table 1 for the cases of $\eta^* \to \infty$ and $\eta^* = 0$, respectively, as they should be. Our collocation results for finite values of $\beta a/\eta$ are found to agree very well with the numerical solutions obtained by using spherical bipolar coordinates (Chen and Keh, 1995). As expected, the results in Table 3 illustrate that the normalized drag force on the particle is a monotonic increasing function of a/b, and will become infinite in the limit $a/b = 1$, for any given value of $\beta a/\eta$. The normalized drag force in general increases with an increase in $\beta a/\eta$ (or with a

Table 3
The normalized drag force F/F_0 experienced by a slip spherical particle translating normal to a single plane wall at various values of a/b and $\beta a/\eta$

a/b	F/F_0			
	$\beta a/\eta = 1$	$\beta a/\eta = 3$	$\beta a/\eta = 10$	$\beta a/\eta = 30$
0.1	1.09203	1.10318	1.11545	1.12194
0.2	1.20202	1.22841	1.25824	1.27436
0.3	1.33571	1.38253	1.43728	1.46776
0.4	1.50256	1.57674	1.66731	1.71979
0.5	1.71919	1.83047	1.97409	2.06195
0.6	2.01769	2.18062	2.40663	2.55550
0.7	2.46968	2.70754	3.07122	3.33704
0.8	3.27889	3.63260	4.25537	4.78768
0.9	5.40032	5.94513	7.18345	8.57327
0.95	9.21176	9.84840	11.85025	14.77138
0.975	16.37460	16.82014	19.54666	24.71630
0.99	37.04963	36.17587	39.16876	48.07314
0.995	70.90285	67.23550	68.98247	80.70473
0.999	338.179	309.2004	291.797	304.0558

decrease in the slip coefficient β^{-1}), keeping a/b unchanged. When the value of a/b is close to unity (say, greater than about 0.975), however, F/F_0 first decreases with an increase in $\beta a/\eta$ from $\beta a/\eta = 0$, reaches a minimum at some finite value of $\beta a/\eta$, and then increases with increasing $\beta a/\eta$ to the limit $\beta a/\eta \to \infty$.

A number of converged collocation solutions for the normalized drag force are presented in Table 4 for the translation of a spherical particle perpendicular to two plane walls at two particular positions between them (with $b/(b+c) = 0.25$ and 0.5) for various values of a/b and $\beta a/\eta$. For the special cases of a no-slip sphere (with $\beta a/\eta \to \infty$) and a perfect-slip sphere (with $\beta a/\eta = 0$), our results are still the same as those presented in Table 2 for the cases of $\eta^* \to \infty$ and $\eta^* = 0$, respectively. Analogous to the situation of translation of a slip sphere normal to a single wall, for a constant value of $b/(b+c)$, Table 4 indicates that the normalized drag force on the particle increase monotonically with an increase in a/b for a fixed value of $\beta a/\eta$ and with an increase in $\beta a/\eta$ for a given value of a/b not too close to unity. Again, $F/F_0 = 1$ as $a/b = 0$ and $F/F_0 \to \infty$ as $a/b \to 1$ for any given values of $b/(b+c)$ and $\beta a/\eta$. It can be found from a comparison among Tables 1–4 that the boundary effects on a slip solid sphere with a finite value of $\beta a/\eta$ is different from those on a spherical fluid droplet with a value of $3\eta^*$ equal to $\beta a/\eta$, although the flow field induced by an isolated slip solid sphere is equivalent to the external flow field caused by an isolated fluid droplet under this condition.

Fig. 4 shows the normalized drag force exerted on a spherical particle with $\beta a/\eta = 10$ normal to two plane walls. At a given value of $2a/(b+c)$, the particle (or a particle with any other value of $\beta a/\eta$, whose collocation results are not exhibited here but can also be obtained accurately) experiences a minimum drag when it is located midway between the two walls as illustrated in Fig. 2. The drag force becomes infinite as the particle touches either of the walls.

In Fig. 5, the normalized drag force for the motion of a spherical particle located midway between two parallel plane walls (with $c = b$) are plotted by solid curves as functions of a/b for various values of $\beta a/\eta$. The corresponding drag on the particle when the second wall is not present (with $c \to \infty$) is also plotted by dashed curves in the same figure for comparison. It can be seen from this figure (or from a comparison between Table 3 and Table 4) that, for an arbitrary combination of parameters a/b and $\beta a/\eta$, the assumption that the results for two walls can be obtained by simple addition of the single-wall effects also gives too large a correction to the hydrodynamic drag force on a particle.

Since the general problem of creeping motion of a particle in an arbitrary direction between two parallel plane walls is linear, its solution can be obtained as the vectorial summation of the solutions for its two subproblems: motion perpendicular to the plane walls, which is examined in this paper, and motion parallel to the walls. The collocation solutions for the slow motion of a slip sphere parallel to two plane walls have already been obtained (Chen and Keh, 2003), and it was found that, in general, the normalized wall-corrected drag force acting on the particle also increases with an increase in the parameter $\beta a/\eta$. A comparison between those results and our solution shows that the plane walls exert the greatest drag force on the particle when motion occurs normal to them, and the smallest in the case of migration parallel to them. Therefore, the direction of creeping motion of a particle in the vicinity of two parallel plane walls is different from that of the applied force, except when it is oriented parallel or perpendicular to the plane walls.

Table 4
The normalized drag force F/F_0 experienced by a slip spherical particle translating normal to two parallel plane walls at various values of a/b, $b/(b+c)$, and $\beta a/\eta$

$b/(b+c)$	a/b	F/F_0			
		$\beta a/\eta = 1$	$\beta a/\eta = 3$	$\beta a/\eta = 10$	$\beta a/\eta = 30$
0.25	0.1	1.09338	1.10471	1.11719	1.12378
	0.2	1.20524	1.23220	1.26263	1.27908
	0.3	1.34161	1.38951	1.44555	1.47676
	0.4	1.51100	1.58812	1.68108	1.73492
	0.5	1.73329	1.84776	1.99538	2.08554
	0.6	2.03770	2.20563	2.43790	2.59042
	0.7	2.49740	2.74243	3.11542	3.38674
	0.8	3.31613	3.67990	4.31599	4.85625
	0.9	5.44933	6.00783	7.26457	8.66552
	0.95	9.26761	9.92007	11.94337	14.87754
	0.975	16.43417	16.89664	19.64627	24.82997
	0.99	37.11149	36.25539	39.27240	48.19151
	0.995	70.96550	67.31606	69.08750	80.82471
	0.999	338.242	309.2819	291.904	304.1771
0.5	0.1	1.12192	1.13710	1.15391	1.16285
	0.2	1.27579	1.31373	1.35721	1.38097
	0.3	1.47365	1.54460	1.62930	1.67720
	0.4	1.73475	1.85273	2.00065	2.08800
	0.5	2.09236	2.27720	2.52319	2.67685
	0.6	2.61052	2.89170	3.29498	3.56642
	0.7	3.43222	3.85676	4.52850	5.02991
	0.8	4.96467	5.61483	6.79865	7.82946
	0.9	9.11767	10.14440	12.55398	15.29669
	0.95	16.69406	17.90183	21.83610	27.64009
	0.975	30.99614	31.82039	37.20293	47.50328
	0.99	72.33189	70.51678	76.43143	94.20090
	0.995	140.0334	132.6311	136.0535	159.4588
	0.999	674.615	616.5868	581.706	606.1816

6. Conclusions

In this work, the slow translational motions of a spherical fluid or solid particle in a viscous fluid perpendicular to two parallel plane walls at an arbitrary position between them are studied theoretically, where the fluid may slip at the particle surface. A semi-analytical method with the boundary collocation technique has been used to solve the Stokes equation for the fluid flow field. The results for the hydrodynamic drag force exerted on the particle indicate that the solution procedure converges rapidly and accurate solutions can be obtained for various cases of the particle's relative viscosity or slip coefficient and of the separation between the particle and the confining boundaries. It has been found that, for given relative positions of the walls, the wall-corrected drag force acting on the particle normalized by the value in the absence of the walls in general is an increasing function of the internal-to-external viscosity ratio or a decreasing function of the dimensionless slip coefficient. For a given particle translating between two parallel plane walls separated by a fixed distance, the particle experiences a minimum drag force when it is located midway between the walls, and the drag force becomes infinite as the particle touches either of the walls.

The hydrodynamic drag force acting on a slip spherical particle migrating parallel to two infinite plane walls at an arbitrary position between them was calculated in previous works (Keh and Chen, 2001; Chen and Keh, 2003) for various values of the parameters η^* or $\beta a/\eta$, a/b, and $b/(b+c)$, and it was also found that the normalized drag force increases with an increase in a/b and in general increases with increasing η^* or $\beta a/\eta$. However, the boundary effect on the motion of a particle is much stronger for the perpendicular migration. For the general problem of a slip particle migrating in an arbitrary direction with respect to the two parallel plane walls, the solution can be obtained by adding both the parallel and transverse results vectorially.

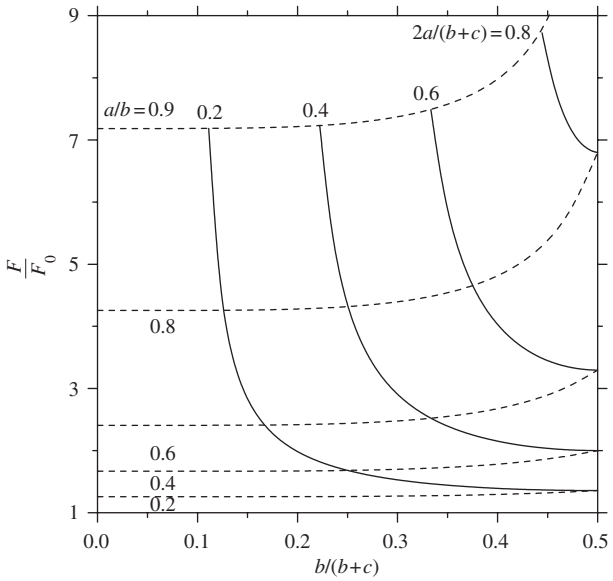

Fig. 4. Plots of the normalized drag force F/F_0 on a slip spherical particle (with $\beta a/\eta = 10$) translating perpendicular to two plane walls versus the ratio $b/(b+c)$ with a/b and $2a/(b+c)$ as parameters.

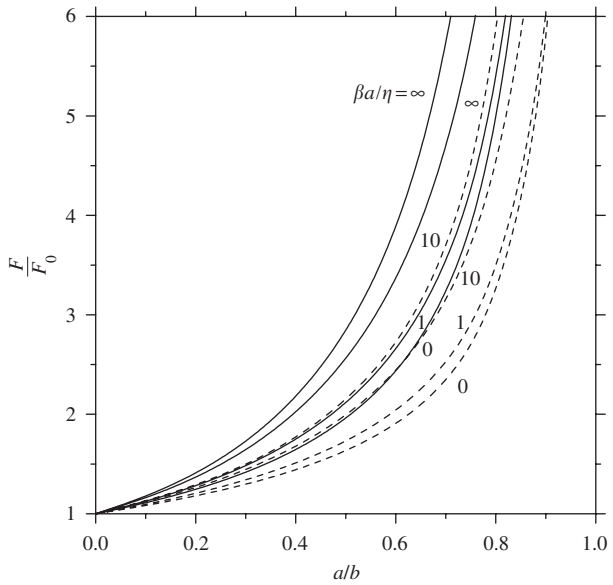

Fig. 5. Plots of the normalized drag force F/F_0 on a slip spherical particle situated midway between two parallel plane walls (with $c = b$) undergoing perpendicular translation versus the ratio a/b with $\beta a/\eta$ as a parameter. The dashed curves are plotted for the translation of an identical particle normal to a single plane wall for comparison.

Acknowledgement

Part of this research was supported by the National Science Council of the Republic of China.

Appendix A. Definitions of some functions in Sections 2 and 4

The functions $\alpha_{in}^{(j)}$ and $\gamma_{in}^{(j)}$ for i and j equal to 1 or 2 in Eqs. (14)–(16) and (19) are defined by

$$\alpha_{in}^{(1)}(r,\theta) = -r^{n+2i-4}\Big[(n+1)G_{n+1}^{-1/2}(\cos\theta)\csc\theta - (2n+2i-3)G_n^{-1/2}(\cos\theta)\cot\theta\Big], \tag{A.1}$$

$$\alpha_{in}^{(2)}(r,\theta) = -r^{n+2i-4}\Big[(2n+2i-3)G_n^{-1/2}(\cos\theta) + P_n(\cos\theta)\Big]; \tag{A.2}$$

$$\begin{aligned}\gamma_{in}^{(1)}(r,\theta) = & -\int_0^\infty \big[G_+''(\sigma,\eta)B_{in}'(\omega,-b) - G_+''(\eta,\sigma)B_{in}'(\omega,c)\\ & -G_+'(\sigma,\eta)B_{in}''(\omega,-b) + G_+'(\eta,\sigma)B_{in}''(\omega,c)\big]\omega \mathrm{J}_1(\omega r\sin\theta)\,\mathrm{d}\omega\\ & - r^{-n+2i-3}\Big[(n+1)G_{n+1}^{-1/2}(\cos\theta)\csc\theta - 2(i-1)G_n^{-1/2}(\cos\theta)\cot\theta\Big],\end{aligned} \tag{A.3}$$

$$\begin{aligned}\gamma_{in}^{(2)}(r,\theta) = & -\int_0^\infty \big[-G_-'(\sigma,\eta)B_{in}'(\omega,-b) + G_-'(\eta,\sigma)B_{in}'(\omega,c)\\ & + G_-''(\sigma,\eta)B_{in}''(\omega,-b) - G_-''(\eta,\sigma)B_{in}''(\omega,c)\big]\omega \mathrm{J}_0(\omega r\sin\theta)\,\mathrm{d}\omega\\ & - r^{-n+2i-3}\Big[P_n(\cos\theta) + 2(i-1)G_n^{-1/2}(\cos\theta)\Big],\end{aligned} \tag{A.4}$$

where

$$B_{1n}'(\omega,z) = -\frac{1}{n!}\left(\frac{\omega|z|}{z}\right)^{n-1}\mathrm{e}^{-\omega|z|}, \tag{A.5}$$

$$B_{1n}''(\omega,z) = -\frac{\omega^{n-1}}{n!}\left(\frac{|z|}{z}\right)^{n}\mathrm{e}^{-\omega|z|}, \tag{A.6}$$

$$B_{2n}'(\omega,z) = -\frac{1}{n!}\left(\frac{\omega|z|}{z}\right)^{n-3}[(2n-3)\omega|z| - n(n-2)]\mathrm{e}^{-\omega|z|}, \tag{A.7}$$

$$B_{2n}''(\omega,z) = -\frac{\omega^{n-3}}{n!}\left(\frac{|z|}{z}\right)^{n}[(2n-3)\omega|z| - (n-1)(n-3)]\mathrm{e}^{-\omega|z|}, \tag{A.8}$$

$$G_\pm'(\mu,v) = \tau^*\mu v(\mu' \pm \tau' v'), \tag{A.9}$$

$$G_\pm''(\mu,v) = \tau^*[v(\cosh\mu - \tau' v') \pm \mu(\mu' - \tau'\cosh v)]; \tag{A.10}$$

$$\mu' = \frac{\sinh\mu}{\mu}, \quad v' = \frac{\sinh v}{v}, \quad \tau' = \frac{\sinh\tau}{\tau}, \quad \tau^* = \frac{\tau}{\sinh^2\tau - \tau^2}, \tag{A.11}$$

$$\sigma = \omega(r\cos\theta + b), \quad \eta = \omega(r\cos\theta - c), \quad \tau = \omega(b+c). \tag{A.12}$$

The functions α_{in}^* and γ_{in}^* for i equal to 1 or 2 in Eqs. (16d) and (19) are defined by

$$\begin{aligned}\alpha_{in}^*(r,\theta) = & -r^{n+2i-5}\Big[(n+1)(n+2i-5)G_{n+1}^{-1/2}(\cos\theta)\cot\theta\\ & -(n+2i-5)(2n+2i-3)G_n^{-1/2}(\cos\theta)\csc\theta\\ & +(5-2i+n\cot^2\theta)P_n(\cos\theta)\sin\theta - nP_{n-1}(\cos\theta)\cot\theta\Big],\end{aligned} \tag{A.13}$$

$$\gamma_{in}^*(r,\theta) = -\cos\theta\,\sin\theta\big[C_{in}^*(r,\theta) + D_{in}^*(r,\theta)\big] - (\cos^2\theta - \sin^2\theta)\big[C_{in}^{**}(r,\theta) + D_{in}^{**}(r,\theta)\big], \tag{A.14}$$

where

$$\begin{aligned}C_{1n}^*(r,\theta) = & -2r^{-(n+2)}\Big[(n+1)(n+\csc^2\theta)G_{n+1}^{-1/2}(\cos\theta) - (3n+2)P_n(\cos\theta)\cos\theta\\ & +nP_{n-1}(\cos\theta)\Big],\end{aligned} \tag{A.15}$$

$$C^{*}_{2n}(r,\theta) = 2r^{-n}\Big[2(2n-1+\cot^2\theta)G_n^{-1/2}(\cos\theta)\cos\theta-(n+1)(n-1+\cot^2\theta)G_{n+1}^{-1/2}(\cos\theta) -(n+2-4\sin^2\theta)P_{n-1}(\cos\theta)+3nP_n(\cos\theta)\cos\theta\Big], \tag{A.16}$$

$$C^{**}_{1n}(r,\theta) = -r^{-(n+2)}\Big\{n\cot\theta\Big[(n+1)G_{n+1}^{-1/2}(\cos\theta)+P_{n-1}(\cos\theta)\Big] +[(3n+2)\sin\theta-n\csc\theta]P_n(\cos\theta)\Big\}, \tag{A.17}$$

$$C^{**}_{2n}(r,\theta) = -r^{-n}\Big\{2[2(n-1)\sin\theta-(n-2)\csc\theta]G_n^{-1/2}(\cos\theta) +(n^2-n-2)G_{n+1}^{-1/2}(\cos\theta)\cot\theta+(n-4\sin^2\theta)P_{n-1}(\cos\theta)\cot\theta +n(3\sin\theta-\csc\theta)P_n(\cos\theta)\Big\}, \tag{A.18}$$

$$D^{*}_{in}(r,\theta) = \int_0^\infty\Big\{\big[G''_+(\sigma,\eta)B'_{in}(\omega,-b)-G''_+(\eta,\sigma)B'_{in}(\omega,c) -G'_+(\sigma,\eta)B''_{in}(\omega,-b)+G'_+(\eta,\sigma)B''_{in}(\omega,c)\big][\mathrm{J}_0(\omega r\sin\theta)-\mathrm{J}_2(\omega r\sin\theta)] +2\big[G^{*}_-(\sigma,\eta)B'_{in}(\omega,-b)-G^{*}_-(\eta,\sigma)B'_{in}(\omega,c) -G^{**}_-(\sigma,\eta)B''_{in}(\omega,-b)+G^{**}_-(\eta,\sigma)B''_{in}(\omega,c)\big]\mathrm{J}_0(\omega r\sin\theta)\Big\}\omega^2\,\mathrm{d}\omega, \tag{A.19}$$

$$D^{**}_{in}(r,\theta) = \int_0^\infty\Big\{\big[G^{**}_+(\sigma,\eta)B'_{in}(\omega,-b)-G^{**}_+(\eta,\sigma)B'_{in}(\omega,c)-G^{*}_+(\sigma,\eta)B''_{in}(\omega,-b) +G^{*}_+(\eta,\sigma)B''_{in}(\omega,c)\big]+\big[G'_-(\sigma,\eta)B'_{in}(\omega,-b)-G'_-(\eta,\sigma)B'_{in}(\omega,c) -G''_-(\sigma,\eta)B''_{in}(\omega,-b)+G''_-(\eta,\sigma)B''_{in}(\omega,c)\big]\Big\}\omega^2\mathrm{J}_1(\omega r\sin\theta)\,\mathrm{d}\omega \tag{A.20}$$

and

$$G^{*}_{\pm}(\mu,\nu) = \tau^{*}[(\mu+\nu)(\mu'\pm\tau'\nu')+\nu(\cosh\mu-\mu')\pm\tau'\mu(\cosh\nu-\nu')], \tag{A.21}$$

$$G^{**}_{\pm}(\mu,\nu) = \tau^{*}[\cosh\mu-\tau'\nu'\pm(\mu'-\tau'\cosh\nu)+\nu\sinh\mu-\tau'(\cosh\nu-\nu') \pm(\cosh\mu-\mu'-\tau'\mu\sinh\nu)]. \tag{A.22}$$

References

Bart, E., 1968. The slow unsteady settling of a fluid sphere toward a flat fluid interface. Chemical Engineering Science 23, 193–210.

Basset, A.B., 1961. A Treatise on Hydrodynamics, vol. 2. Dover, New York.

Brenner, H., 1961. The slow motion of a sphere through a viscous fluid towards a plane surface. Chemical Engineering Science 16, 242–251.

Brenner, H., 1971. Pressure drop due to the motion of neutrally buoyant particles in duct flows. II. Spherical droplets and bubbles. Industrial and Engineering Chemistry, Fundamentals 10, 537–542.

Chen, P.Y., Keh, H.J., 2003. Slow motion of a slip spherical particle parallel to one or two plane walls. Journal of the Chinese Institute of Chemical Engineers 34, 123–133.

Chen, S.H., Keh, H.J., 1995. Axisymmetric motion of two spherical particles with slip surfaces. Journal of Colloid and Interface Science 171, 63–72.

Coutanceau, M., Thizon, P., 1981. Wall effect on the bubble behaviour in highly viscous liquids. Journal of Fluid Mechanics 107, 339–373.

Davis, M.H., 1972. Collisions of small cloud droplets: gas kinetic effects. Journal of Atmospheric Science 29, 911–915.

Ganatos, P., Weinbaum, S., Pfeffer, R., 1980. A strong interaction theory for the creeping motion of a sphere between plane parallel boundaries. Part 1. Perpendicular motion. Journal of Fluid Mechanics 99, 739–753.

Hadamard, J.S., 1911. Mouvement permanent lent d'une sphere liquid et visqueuse dans un liquide visqueux. Comptes Rendus Hebdomadaires des Seances de V, Académie des Sciences (Paris) 152, 1735–1738.

Happel, J., Brenner, H., 1983. Low Reynolds Number Hydrodynamics. Nijhoff, The Netherlands.

Hetsroni, G., Haber, S., Wacholder, E., 1970. The flow fields in and around a droplet moving axially within a tube. Journal of Fluid Mechanics 41, 689–705.

Ho, B.P., Leal, L.G., 1974. Inertial migration of rigid spheres in two-dimensional unidirectional flows. Journal of Fluid Mechanics 65, 365–400.

Hutchins, D.K., Harper, M.H., Felder, R.L., 1995. Slip correction measurements for solid spherical particles by modulated dynamic light scattering. Aerosol Science and Technology 22, 202–218.

Keh, H.J., Chang, J.H., 1998. Boundary effects on the creeping-flow and thermophoretic motions of an aerosol particle in a spherical cavity. Chemical Engineering Science 53, 2365–2377.

Keh, H.J., Chen, P.Y., 2001. Slow motion of a droplet between two parallel plane walls. Chemical Engineering Science 56, 6863–6871.

Keh, H.J., Chen, S.H., 1997. Low-Reynolds-number hydrodynamic interactions in a suspension of spherical particles with slip surfaces. Chemical Engineering Science 52, 1789–1805.

Keh, H.J., Tseng, Y.K., 1992. Slow motion of Multiple droplets in arbitrary three-dimensional configurations. A.I.Ch.E. Journal 38, 1881–1904.

Kennard, E.H., 1938. Kinetic Theory of Gases. McGraw-Hill, New York.

Loyalka, S.K., 1990. Slip and jump coefficients for rarefied gas flows: variational results for Lennard-Jones and $n(r)-6$ potentials. Physica A 163, 813–821.

Lu, S.Y., Lee, C.T., 2001. Boundary effects on creeping motion of an aerosol particle in a non-concentric pore. Chemical Engineering Science 56, 5207–5216.

Lu, S.Y., Lee, C.T., 2002. Creeping motion of a spherical aerosol particle in a cylindrical pore. Chemical Engineering Science 57, 1479–1484.

Maude, A.D., 1961. End effects in a falling-sphere viscometer. British Journal of Applied Physics 12, 293–295.

O'Brien, V., 1968. Form factors for deformed spheroids in Stokes flow. A.I.Ch.E. Journal 14, 870–875.

Reed, L.D., Morrison, F.A., 1974. Particle interactions in viscous flow at small values of Knudsen number. Journal of Aerosol Science 5, 175–189.

Rushton, E., Davies, G.A., 1973. The slow unsteady settling of two fluid spheres along their line of centers. Applied Scientific Research 28, 37–61.

Rybczynski, W., 1911. Uber die fortschreitende bewegung einer flussigen kugel in einem zahenmedium. Bulletin de l'Académie des Sciences de Cracovie, Series A 1, 40–46.

Shapira, M., Haber, S., 1988. Low Reynolds number motion of a droplet between two parallel plates. International Journal of Multiphase Flow 14, 483–506.

Stokes, G.G., 1851. On the effect of the internal friction of fluid on pendulums. Transactions of the Cambridge Philosophical Society 9, 8–106.

Talbot, L., Cheng, R.K., Schefer, R.W., Willis, D.R., 1980. Thermophoresis of particles in heated boundary layer. Journal of Fluid Mechanics 101, 737–758.

Wacholder, E., Weihs, D., 1972. Slow motion of a fluid sphere in the vicinity of another sphere or a plane boundary. Chemical Engineering Science 27, 1817–1828.

Ying, R., Peters, M.H., 1991. Interparticle and particle-surface gas dynamic interactions. Aerosol Science and Technology 14, 418–433.